Wave-function mapping conditions in open quantum dot structures

M. Mendoza and P. A. Schulz
Instituto de Física Gleb Wataghin, UNICAMP, Caixa Postal 6165, 13083-970, Campinas, São Paulo, Brazil
(Received 23 August 2002; revised manuscript received 15 January 2003; published 5 November 2003)

We discuss the minimal conditions for wave-function spectroscopy, using resonant tunneling as the measurement tool, in open quantum dots. The present results establish a parameter region where the wave-function spectroscopy by resonant tunneling can be achieved. A breakdown of the mapping condition is related to a change into a double quantum dot structure induced by the local probing potential. The precise control over shape and extension of the potential probes is irrelevant for wave-function mapping. Moreover, the present system is a realization of a tunable Fano system beyond the wave-function mapping regime, as well as a system where the states can be selectively manipulated.

DOI: 10.1103/PhysRevB.68.205302 PACS number(s): 73.40.Gk, 73.21.Fg, 73.21.La

I. INTRODUCTION

Experimental probing of electronic states in systems showing spatial quantization is probably the most direct visualization of quantum-mechanical effects. Such probing in condensed matter has been a challenge over decades until the development of artificial model structures, initially semiconductor quantum wells and more recently quasi-one- (or zero-) dimensional mesoscopic systems. The control over the design and fabrication of these structures leads naturally to the introduction of well-defined local probes of the electronic states. A landmark in the wave-function spectroscopy is the optical probing of quantum-well eigenstates by Marzin and Gerard more than 10 years ago.[1] The basic idea introduced in this work is that a very thin barrier, which can therefore be considered as a δ function, is grown within the quantum well at a certain position, leading to a potential perturbation of the form $V\delta(z-z_0)$. Such perturbation probes the probability density at z_0 by means of the eigenvalues E_i shifts, which in first-order approximation are simply

$$E_i' = E_i + V|\Psi_i(z_0)|^2. \tag{1}$$

In the work by Marzin and Gerard, these energy shifts were obtained by photoluminescence measurements performed in a set of nominally identical quantum wells but with the perturbative barrier located at different positions. In other words, such mappings rely on measurements performed on different samples, each one probing the wave function at a designed position. Later on, Salis and co-workers[2] performed a wave-function spectroscopy on a single parabolic quantum well, where the electron distribution was displaced with respect to a fixed perturbative barrier by applying an electric field. The energy shifts were obtained now by magnetotransport measurements. The great advantage of this procedure, namely, the spectroscopy on a single sample, is somehow eclipsed by the fact that only a specific system (parabolic quantum wells) is suitable for it. A variation of this spectroscopy is the introduction of monolayers with magnetic ions embedded in different positions of a quantum well, using the Zeeman splitting as a probe for the wave function.[3] An alternative approach, based on energy shifts measured by means of resonant tunneling, has been proposed also a few years ago.[4] Now the mapping of the probability density along the quantum well is related to shifts of the resonant tunneling current peaks for an ensemble of double-barrier tunneling diodes, where each sample has a perturbative potential spike located at a specific position. This tunneling wave-function spectroscopy has not yet been experimentally verified. Nevertheless, magnetotunneling has been used as a tool for imaging of electron wave functions in self-assembled quantum dots.[5]

Imaging of wave functions, in spite of the efforts mentioned above, has experienced a growing interest mainly due to the use of scanning probe microscopes in searching local electron distributions in mesoscopic systems. Within an already long list of achievements, it is worth mentioning the study of Bloch wave functions in quasi-one-dimensional systems, such as single wall carbon nanotubes[6] and imaging of bound states in quantum corrals.[7] In both cases scanning tunneling microscopes were used. Closely related to the approaches using perturbative potential spikes is the use of atomic force microscopes with the measurement of shifts in the conductance across a mesoscopic system as a function of the position of the potential perturbation induced by the atomic force microscope (AFM) tip. An interesting application of this method is the imaging of coherent electron flow from a quantum point contact.[8]

In the present work we analyze the suitability of such imaging procedure for quasibound states in open quantum dot (OQD) system in the resonant tunneling regime. It can be considered the two-dimensional counterpart of the probing of quasibound states in double-barrier quantum wells, considered as a toy model. Here we are mainly interested in the conditions that maximize the energy shift of the resonances in the transmission probability, which can be established without breaking the perturbative regime within the mapping of the wave function. In the present situation we are dealing with the quasibound states of a double point contact in the resonant tunneling regime, a rather different situation from single quantum point contacts,[8] theoretically discussed within a similar framework.[9] Although our main concern is the mapping of quantum dot states, related to resonance shifts in energy, the analysis could also be extended to the behavior of the transmission probability plateaus related to the quantum point contact channels.[10]

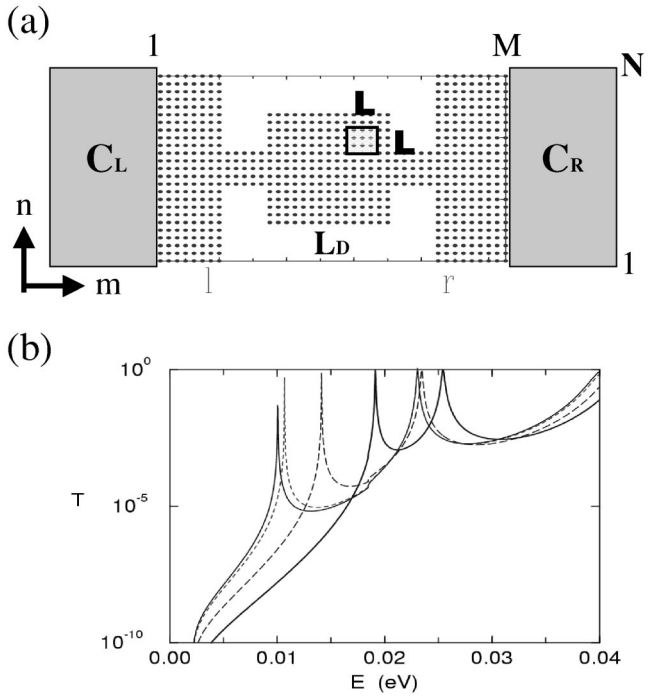

FIG. 1. (a) Schematic illustration of the open quantum dot structure. (b) Total transmission probabilities as functions of incident energy for the structure in (a): bare structure (thin solid line), with a potential bump at the center of the structure with $H=0.05$ eV and $L=1a$ (dashed line), $L=3a$ (long dashed line), and $L=5a$ (thick solid line).

An important point in the present work is that, if a wave function mapping could be experimentally achieved, the OQD system coupled to an AFM tip would be a realization of a tunable Fano system. Fano resonances have been recently observed in electronic transport through a single-electron transistor,[11] but a tunability of the effect has been reached only in the presence of magnetic fields,[12] with the quantum dot in an Aharonov-Bohm interferometer. The degree of freedom introduced by the movable AFM tip opens a new possibility for such tuning in the absence of magnetic-field effects. Although Fano resonances have been discussed before in the context of mesoscopic systems, the present work proposes a possible experimental realization of former theoretical predictions.[13]

II. IMAGING OF WAVE FUNCTIONS IN OPEN QUANTUM DOTS

A. Model calculation

The transmission probabilities through an OQD are calculated within a Green's-function formalism applied to a lattice model in the tight-binding approximation. This method has already been described throughout the literature and has been applied in a variety of problems in the context of mesoscopic systems.[14–16] For the sake of clarity this method is briefly sketched below.

The OQD structure, emulated by a tight-binding lattice model is depicted in Fig. 1(a). The black circles represent the lattice sites that define a square quantum dot connected to two-dimensional contacts to the left and to the right by point contacts. The size of the quantum dot is $S_{QD}=15a\times 15a$, where a is the host-lattice parameter. The circles inside a square represent a potential column simulating the perturbation induced, for instance, by an AFM tip located on the sample at that position. In what follows we consider perturbations of a single host-lattice site, which corresponds to an extension relative to the quantum dot area of $S_P\approx 4.5\times 10^{-3}S_{QD}$, up to a 5×5 square, corresponding a relative extension of $S_P\approx 0.1S_{QD}$.

It should be kept in mind that lattice models, with nearest-neighbor interactions only, are usually thought as simple, although useful, approximations for superlattices or arrays of quantum dots, where each quantum well or quantum dot is represented by a site of the lattice. Apart from this extreme lattice limit, lattice models are also useful in emulating the bottom of semiconductor conduction bands that are well described by the effective-mass approximation. In the present work, the tight-binding hopping parameter is chosen in order to emulate the electronic effective mass for the GaAs bottom of the conduction band, $m^*=0.067m_0$. Since $V_{x,y}=-\hbar^2/(2m^*a^2)$, $V_{x,y}=0.142$ eV for a lattice parameter of $a=20$ Å. Such parametrization represents quantum dots with lateral sizes up to $L_D=300$ Å, Fig. 1(a), still an order of magnitude lower than the typical dimensions of actual quantum dots constructed by lithographic methods. However, the present results have the intention of illustrating the probing of the local probability density and the relevant scale is the ratio between the extension of the perturbative spike and the dot dimension, S_P/S_{QD}.

The AFM tip can also be seen as a controllable impurity in a quantum dot and therefore a simple tunable experimental realization of a multiply connected nanostructure.[17] In the present approach, a continuous system is discretized into a tight-binding lattice, considering a single s-like orbital per site and only nearest-neighbor hopping elements. These two parameters are the only ones necessary for describing the electronic behavior in laterally modulated heterostructures near the bottom of the GaAs conduction band. The device region of an open quantum dot system modeled this way, Fig. 1(a), is $M=45$ sites long and $N=25$ sites wide. The total Hamiltonian, H_T, is a sum of four terms: the dot and the two point contact regions, described by the H_D, and the left and right contact regions, H_L and H_R, respectively, and the coupling term between the contacts and the dot structure, V:

$$H_T=H_D+H_L+H_R+V. \tag{2}$$

We are interested in the transmission $t_{\nu,\nu'}$ and reflexion $r_{\nu,\nu'}$ amplitudes, related to the $G^+(\nu',r,\nu,l,E)$ and $G^+(\nu',l,\nu,l,E)$ Green's functions, respectively. Here, $l(r)$ stands for a site column at the left (right) of the OQD device, as indicated in Fig. 1(a), while $\nu(\nu')$ are transverse incident (scattered) modes in the contacts at a given energy E. The first step is calculating Green's functions of the semi-infinite contacts C_L and C_R:

$$G^{+}(E)=\sum_{\nu,\mu}\frac{|\psi^{\nu\mu}\rangle\langle\psi^{\nu\mu}|}{E-E^{\nu\mu}+i\eta}, \tag{3}$$

where $|\psi^{\nu\mu}\rangle$ and $E^{\nu\mu}$ are the eigenstates and eigenvalues of the contact regions, with $\nu(\mu)$ as transverse (longitudinal) quantum numbers. Actually, we need the matrix elements of Green's functions for the l and r site columns, given by

$$G_{l(r)}(n,n')=\sum_{\nu=1}^{N}\chi_n^{\nu}(\chi_{n'}^{\nu})^{*}\frac{e^{i\theta_\nu}}{|V_x|}; \tag{4}$$

with

$$\theta_\nu=\cos^{-1}\left[\frac{(E-\epsilon_\nu)}{2V_x}+1\right] \tag{5}$$

and

$$\chi_n^{\nu}=\sqrt{\frac{2}{N+1}}\sin\left(\frac{\pi\nu n}{N+1}\right). \tag{6}$$

The device region can be decoupled in M transverse chains with N sites each. The Hamiltonian for one of these chains i is written as

$$H_i=\sum_{n=1}^{N}(|i,n\rangle\epsilon_{in}\langle i,n|+|i,n\rangle V_{n,n+1}\langle i,n+1| + |i,n\rangle V_{n,n-1}\langle i,n-1|), \tag{7}$$

where the hopping elements at the edges are $V_{N,N+1}=V_{1,0}=0$. The corresponding Green's function is

$$G_i=[(E+i\eta)\mathbf{I}-H_i]^{-1}. \tag{8}$$

Green's functions $G^{+}(\nu',r,\nu,l,E)$ and $G^{+}(\nu',l,\nu,l,E)$ are calculated by means of a recursive procedure, coupling Green's functions of successive transversal chains along the device, Eq. (8), based on the Dyson equation

$$G=G_0+G_0VG=G_0+GVG_0. \tag{9}$$

The starting point of this iterative procedure is Green's function, given by Eq. (4), corresponding to a transversal chain at the right, $r=M+1$ (G_r), of the OQD structure, successively coupled to the device chains G_i and finally to the left contact G_l.

The transmitted and reflected amplitudes are

$$t_{\nu\nu'}(E)=i2|V_x|\sqrt{\sin\theta_{\nu'}\sin\theta_\nu}e^{i(\theta_{\nu l}-\theta_{\nu' r})}G^{+}(\nu',r,\nu,l,E) \tag{10}$$

and

$$r_{\nu\nu'}(E)=i\sqrt{\frac{\sin\theta_{\nu'}}{\sin\theta_\nu}}e^{i(\theta_\nu+\theta_{\nu'})l} \times[2|V_x|\sin\theta_\nu G^{+}(\nu',l,\nu,l,E)+i\delta_{\nu'\nu}]. \tag{11}$$

The total transmission probability, the quantity discussed in what follows, is given by the Landauer-Büttiker formula:

$$T(E)=\sum_{\nu'}^{N}\left(\sum_{\nu}^{N}|t_{\nu'\nu}(E)|^2\right). \tag{12}$$

B. Numerical results: Energy shifts and imaging

The main limitations of resonant tunneling mapping of the wave function, namely, the broadness of measured I-V characteristics, as well as the uncertainties related with a procedure involving a set of different samples,[4] can be overcome in the imaging of quasibound states in OQD's. The embedded potential spikes are substituted by the potential bumps induced by an AFM tip scanned over a single sample and the resonant tunneling current, a rather wide integration of transmission probability resonances, is reduced to single and well defined conductance peaks. Although imaging of coherent electron flow through a quantum point contact has been reported,[8] where the mapping is achieved by measuring deviations of the quantized conductance plateaus as a function of AFM tip position, the use of energy shifts of conductance peaks to image the wave function inside a quantum dot remains to be properly discussed.

Typical transmission probabilities as functions of incident energy are shown in Fig. 1(b). Here we clearly see two resonances due to quasibound states in the quantum dot below the threshold of the first quantized conductance plateau due to the quantum point contacts that connect the dot to the left and right two-dimensional reservoirs. The thin continuous line is for the unperturbed quantum dot. The other curves are for potential bumps at the center of the dot with $H=0.05$ eV, but different sizes. It should be noticed that this is actually a strong perturbation, since the energy separation between the two resonances in the bare dot is ≈ 0.01 eV. The dashed line is for a δ-function-like bump, with $L=1a$. It can be seen that a small shift occurs for the lowest resonance, while the second one remains unchanged as expected. The long-dashed curve is for a wider bump, $L=3a$, with corresponding larger shifts of the resonances. The thick continuous line is for $L=5a$ revealing the signature of a doublet resonance of a symmetrically structured dot, instead of slightly perturbed single quantum dot levels.

The mapping of the probability density is obtained by scanning the potential bump across the quantum dot in both directions. This procedure introduces asymmetries in the structure as far as the perturbation is not at the center of the structure. However, the figure of merit is the position in energy of the transmission resonances and not the peak heights. For the perturbation strength in the results shown in Fig. 1(b), the mapping should be taken carefully. Indeed, such a high perturbation potential, $H=50$ meV, strongly affects the transmission channels when placed near the quantum point contacts. This is illustrated in Fig. 2, where the energy shifts of the lowest and second resonances are depicted as a function of the position of two different perturbative bumps. Figure 2(a) represents a bona fide mapping of the probability densities for a very low, although spatially extended, perturbation: $H=5$ meV and $L=5a$, while Fig. 2(b) shows an inadequate mapping for $H=50$ meV and $L=3a$. The cusps in Fig. 2(b) are artifacts due to mode couplings and show no

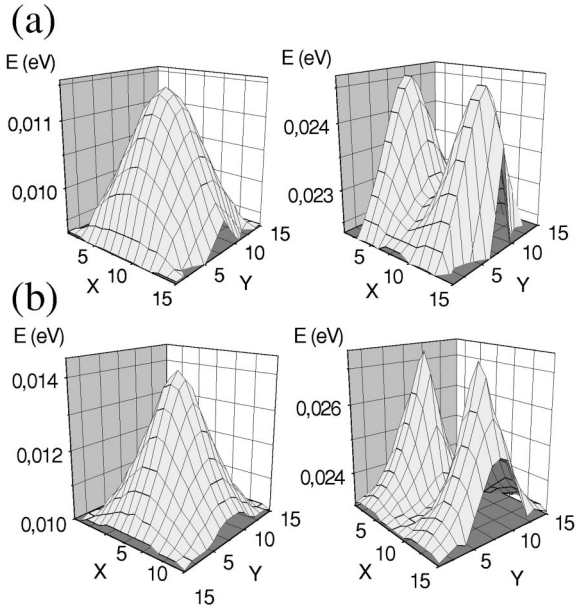

FIG. 2. Energy shifts of the lowest (left) and second (right) quasibound states as a function of the position of the potential bump inside the open quantum dot structure. (a) Bona fide probability density mapping for a wide and low probe potential: $H=5$ meV and $L=5a$. (b) Unrealistic mapping for a high probe potential: $H=50$ meV and $L=3a$.

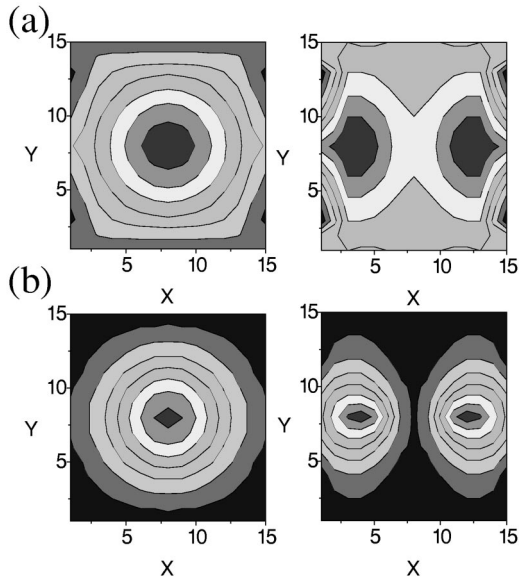

FIG. 3. Contour plots of energy shifts, corresponding to the situations depicted in Fig. 2. The structure probed is an open quantum dot one and in (a), corresponding to a bona fide mapping, the contours indicate finite probability density in the contact regions. (b) High probe potentials isolate the quantum dot.

resemblance with the actual shapes of probability density maxima, while the behavior of the energy shifts in Fig. 2(a) is qualitatively in agreement with the probability densities for the two lowest states of the unperturbed OQD system.

The differences between a fair and an inadequate mapping situation become clearer by looking at the contour plots of the energy shifts as a function of the probing potential position, Fig. 3, for the same cases shown in Fig. 2. In Fig. 3(a) we see a fair mapping for quasibound states in an OQD with a high probability density leaking into the quantum point contacts. This is not the case in Fig. 3(b), where the height of the potential bump, when positioned near the quantum point contacts, strongly suppresses the resonant tunneling channels, turning the open system into a closed one. An appropriate mapping is also obtained for a even wider, $L=7a$, low potential bump ($H=5$ meV) (not shown here). The interesting point here is that the lateral size of the perturbative bump is almost half of the lateral size of the quantum dot being probed, corresponding to a bump to dot area ratio of $S_P \approx 0.2 S_{QD}$. Therefore, the upper limit for the spatial extension of the probing potential is not crucial, as far as the corresponding height of the potential is kept low enough, i.e., $H<E_2-E_1$.

The important finding is that such wave-function mapping should be experimentally feasible, since the perturbation strength can be smoothly tuned in observing the conductance peak shifts,[18] while the actual underlying potential profile—experimentally lesser known—plays no essential role.

III. TUNABLE FANO RESONANCES

As pointed out in the Introduction, if a wave-function mapping could be experimentally achieved, the OQD coupled to an AFM tip would be a realization of a tunable Fano system for a parameter region beyond the mapping condition. Fano resonances have been observed in electronic transport through a quantum dot,[11] but a completely tunable resonance has been reached only with the quantum dot in an Aharonov-Bohm interferometer.[12] The variation of the connecting channels, achievable by changing gate voltages, may provide a partial tunability,[11] but an extra degree of freedom, introduced by the movable AFM tip, allows such tuning in the absence of magnetic-field effects.

The richness of the new effects due to this extra degree of freedom is illustrated by calculations done for OQD structure similar to the one discussed above. Some important aspects are recalled in the inset of Fig. 4(a). The black circle represents a potential column simulating the local induced perturbation. We consider perturbations of a single host-lattice site S_p, which corresponds to an extension relative to the quantum dot of $S_p/S_{QD} \approx 0.02$ for OQD with dimensions $Lx=Ly=7a$. The repulsive perturbation will be characterized by a height H in the range between $H=50$ meV and $H \approx 1$ eV, since now we are not restricted to the mapping condition. A partial tunability of the system, by means of changing the lead widths, is shown in Fig. 4(a). For $w=3a$ (continuous line) we clearly see resonances in the transmission probability due to the bound states of the OQD, as well as the first conductance plateau. For wider leads, $w=5a$ (dashed line), we see the resonances due to OQD states shifted to lower energies, since the effective confinement is diminished with the widening of the contacts. Moreover the resonance peaks are broadened because the coupling to the reservoirs is enhanced. As expected, the conductance plateaus are also shifted to lower energies and the onset of a second plateau can be seen in the same energy range. Two

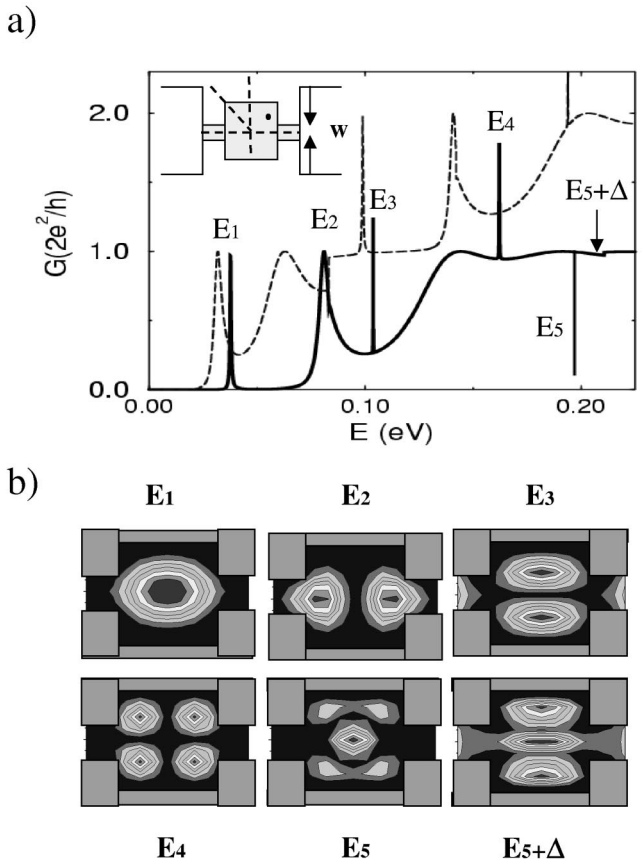

FIG. 4. (a) Conductance for the OQD for $w=3a$, continuous line, and $w=5$, dashed line. Inset: schematic illustration of the open quantum dot structure. (b) Local density of states (probability densities) for the energies labeled in (a), referring to the $w=3a$ case.

aspects related to widening the leads should be kept in mind: (i) the shift in energy and broadening of the resonances are not a monotonous function of the energy; and (ii) even the shape of a resonance may be qualitatively changed, as can be seen for the antiresonance for $w=3a$ changing into a peak for $w=5a$.

The above discussion summarizes the effects on the conductance that can be achieved by varying (symmetrically) the leads, i.e, the voltages of the gate electrodes that actually define the quantum dot structure. In what follows we focus on the new degree of freedom in manipulating dot states. Such new mechanism is introduced by a local potential perturbation that could be moved across the sample, such as an AFM tip, as suggested above. The novelty of this local perturbation is that the resonances may be selectively tuned, exploring the wave-function symmetries of the states.

In order to explore the wave-function symmetries, one has to look along three symmetry axes of the square QD: along the axis connecting the leads (x axis), the axis perpendicular to the line joining the leads and crossing the center of the dot (y axis), and a diagonal, also crossing the center, as indicated in the sketch shown in Fig. 4(a). The shift in energy of a certain resonance peak depends on the position of the local perturbation, since such shift is proportional to the wave-function amplitude at this position, Eq. (1).

Fig. 4(b) shows contour plots of the local density of states at the energies of the four resonances and the antiresonance shown in Fig. 4(a) for the $w=3a$ wide leads case (continuous line). The last panel is for an energy slightly above the antiresonance. Having these contour plots in mind it is straightforward to see that the width of the resonance peak is proportional to the wave-function amplitude leaking into the leads. Of particular interest is the strong localization of the fifth state, which corresponds to the antiresonance in Fig. 4(a), as well as the clear one-dimensional(1D) channel character at off resonance energies in the conductance plateau, $E_5+\Delta$.

Within this framework we are able to understand the effects of the position dependent perturbation. In this sense, two important effects are shown in Fig. 5. First, for a perturbative spike positioned at the center of the quantum dot, Fig. 5(a), we see the selective shift of the resonances in the perturbed system with $H=0.2$ eV(continuous line) compared to the unperturbed one (dashed line). We clearly identify that important shifts (lowest resonance and antiresonance) occur only for those states that have significant amplitude at the center of the dot. Next, for a perturbation $H=0.5$ eV placed at one of the leads (continuous line), Fig. 5(b), no energy shifts of the resonances are observed. On the other hand, a strong suppression of the conductance plateau can be observed, an effect which has been used recently for imaging the electron flow through quantum point contacts.[8]

The dependence of the selective resonance shifts on the wave-function symmetries for moving the perturbative spike along the y axis can be analyzed by comparing Figs. 5(a) and 5(c). Now, for $H=0.05$ eV (continuous line) and $H=4$ eV (dashed line), the second resonance remains almost unchanged and the lowest one is shifted, as expected from the density of states in Fig. 4(b). Having Fig. 4(b) in mind, it is also expected that the third resonance would be perturbed in this situation and, indeed, this resonance is not only shifted in energy but the line shape also changes into a Fano-like form. The perturbation breaks the symmetry of the state, inducing a coupling to the lowest lead state. Moving the perturbation further away from the center in the y direction, Fig. 5(d), this third resonance evolves towards a symmetric peak again (continuous line for $H=0.05$ eV), illustrating the tunability of a specific resonance with a controllable perturbation.

The symmetry of the localized states in the QD gives rise to two new consequences when the perturbation is moved along the diagonal, see Fig. 6. Here dashed and continuous lines are for perturbative spikes at the center and at the diagonal, respectively. Both situations are for $H=0.5$ eV. First, we observe the inversion of the Fano resonance associated to E_3:[13] from Fig. 5(c) to Fig. 6, the peak position is reversed. Moreover, only an off center perturbation along the diagonal breaks the symmetry of the E_4 state, allowing the coupling to the 1D channel and leading to a Fano resonance. This symmetry is not broken with the perturbation positioned along the other symmetry axes (x and y), since the density of states related to E_4 is negligible there.[19]

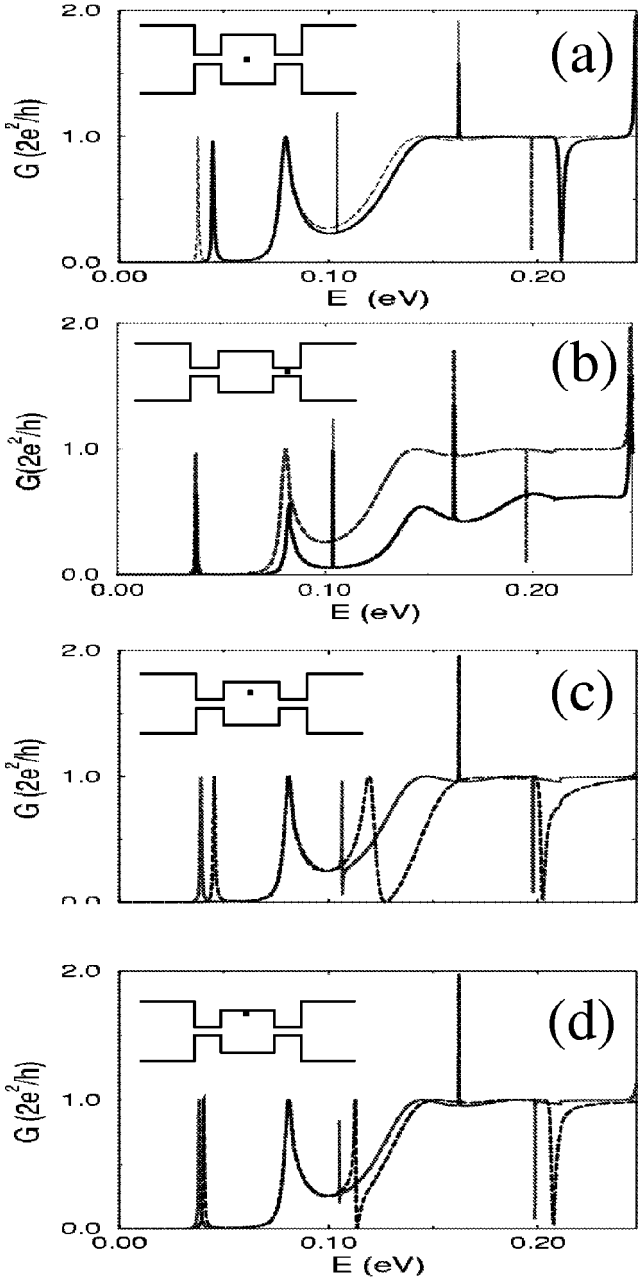

FIG. 5. Total transmission probabilities (conductance) for the OQD as a function of incident electron energy, comparing the unperturbed with perturbed ones at the positions indicated in the insets. (a) Dashed line for $H=0.0$ eV and continuous line for $H=0.2$ eV. (b) Dashed line for $H=0.0$ eV: and continuous line for $H=0.5$ eV. (c) and (d) Continuous line for $H=0.05$ eV and dashed line for $H=4$ eV.

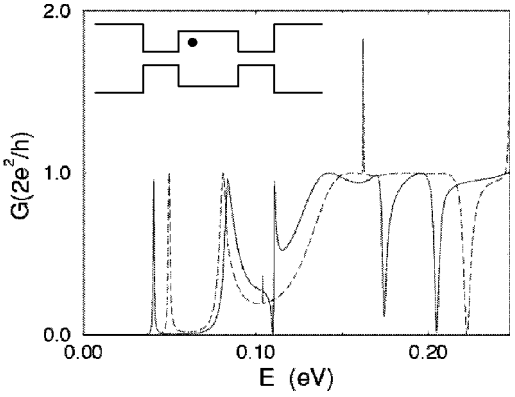

FIG. 6. Conductance for the OQD as a function of incident electron energy for a perturbative spike at the center of the dot (dashed line) and near a corner (continuous line). For both cases $H=0.5$ eV.

IV. FINAL REMARKS

The present work addresses the modeling of wave-functions imaging by means of experimental perturbative approaches. The situation studied here concerns a two-dimensional problem, namely, an OQD in the resonant tunneling regime. The present discussion applies to devices with highly transmitting channels, making the number of electrons in the dot an ill-defined quantity, in contrast to systems where the single-electron charging effects are important. Charging effects are crucial in other mapping experiments, such as the imaging of incompressible stripes in the quantum Hall regime[20] in which a different scenario is revealed with dramatic charging effects induced by the scanning probe. In absence of magnetic fields, however, such effects are drastically minimized.[21] In the situation considered here, single-particle resonances should also be robust with respect to the effects of electron-electron interactions. The important point is the comparison between the conductances of a unperturbed and the perturbed OQD and the perturbation should not influence the number of electrons in the structure. OQD structures with such characteristics have been under investigation previously[22] and are candidates for the wave-function mapping of the low-lying resonances focused in the present study.

Wave-function mapping is achievable with rather spatially extended perturbative movable potentials. The opposite limit, namely, higher resonances with shorter de Broglie wavelengths, has been recently considered for the semiclassical limit by means of a microwave analog to an OQD.[23]

This is contrary to the initial idea of δ-like perturbative spikes,[1,2] but provides a strong support to the imaging using AFM induced perturbations, where the exact form and extension of the depletion underneath the tip are not so clearly controlled. We believe that our results open new possibilities for the imaging experiments carried out so far on single quantum point contacts,[8] as well as for the quest for selective manipulation of quantum states. An OQD coupled to the tip of an AFM could also be a new realization of tunable resonance line shapes of the conductance through mesoscopic systems.

ACKNOWLEDGMENTS

M.M. would like to acknowledge the Brazilian agency CAPES for financial support, while P.A.S. is grateful for the continuous support provided by FAPESP.

[1] J-Y. Marzin and J-M. Gérard, Phys. Rev. Lett. **62**, 217 (1989).
[2] G. Salis, B. Graf, K. Ensslin, K. Campman, K. Maranowski, and A.C. Gossard, Phys. Rev. Lett. **79**, 5106 (1997).
[3] G. Yang, J.K. Furdyna, and H. Luo, Phys. Rev. B **62**, 4226 (2000).
[4] A. Nogueira and A. Latgé, Phys. Rev. B **57**, 1649 (1998).
[5] E.E. Vdovin, A. Levin, A. Patane, L. Eaves, P.C. Main, Yu.N. Khanin, Yu.V. Dubrovskii, M. Henini, and G. Hill, Science **290**, 122 (2000).
[6] S.G. Lemay, J.W. Janssen, M. van den Hout, M. Mooij, M.J. Bronikowski, P.A. Willis, R.E. Smalley, L.P. Kouwenhoven, and C. Dekker, Nature (London) **412**, 617 (2001).
[7] M.F. Crommie, C.P. Lutz, and D.M. Eigler, Science **262**, 218 (1993).
[8] M.A. Topinka, B.J. LeRoy, S.E.J. Shaw, E.J. Heller, R.M. Westervelt, K.D. Maranowski, and A.C. Gossard, Science **289**, 2323 (2000).
[9] G-P. He, S-L. Zhu, and Z.D. Wang, Phys. Rev. B **65**, 205321 (2002).
[10] A.R. Rocha and J.A. Brum, Braz. J. Phys. **32-2A**, 296 (2002).
[11] J. Göres, D. Goldhaber-Gordon, S. Heemeyer, M.A. Kastner, H. Shtrikman, D. Mahalu, and U. Meirav, Phys. Rev. B **62**, 2188 (2000).
[12] K. Kobayashi, H. Aikawa, S. Katsumoto, and Y. Iye, Phys. Rev. Lett. **88**, 256806 (2002).
[13] C.S. Kim, A.M. Satanin, Y.S. Joe, and R.M. Cosby, Phys. Rev. B **60**, 10 962 (1999).
[14] David K. Ferry and Stephen M. Goodnick, *Transport in Nanostructures* (Cambridge University Press, Cambridge, 1997), p. 156.
[15] F. Sols, M. Macucci, U. Ravaioli, and K. Hess, J. Appl. Phys. **66**, 3892 (1989).
[16] S. Datta, Superlattices Microstruct. **28**, 253 (2000).
[17] Y.S. Joe, R.M. Cosby, M.W.C. Dharma-Wardana, and S.E. Ulloa, J. Appl. Phys. **76**, 4676 (1994).
[18] One should remind that the conductance peaks of the unperturbed system deliver the appropriate energy scale.
[19] S.-J. Xiong and Y. Yin, Phys. Rev. B **66**, 153315 (2002).
[20] G. Finkelstein, P.I. Glicofridis, R.C. Ashoori, and M. Shayegan, Science **289**, 90 (2000).
[21] G. Finkelstein, P.I. Glicofridis, S.H. Tessmer, R.C. Ashoori, and M.R. Melloch, Physica E (Amsterdam) **6**, 251 (2000).
[22] T. Lundberg, J.E.F. Frost, K.-F. Berggren, Z.-L. Ji, C.-T. Liang, I.M. Castleton, D.A. Richie, and M. Pepper, Semicond. Sci. Technol. **12**, 875 (1997).
[23] Y.-H. Kim, M. Barth, U. Kuhl, H.-J. Stöckmann, and J.P. Bird, Phys. Rev. B **68**, 045315 (2003).